Studies on the mechanism of action of antitumor bis(aminophenolate) ruthenium(III) complexes

Orsolya Dömötör[a,b], Rodrigo F. M. de Almeida[c], Leonor Côrte-Real[d], Cristina P. Matos[d,e], Fernanda Marques[f], António Matos[g], Carla Real[c], Tamás Kiss[a,b], Éva Anna Enyedy[a], M. Helena Garcia[d], Ana Isabel Tomaz[d]∗

[a] Department of Inorganic and Analytical Chemistry, University of Szeged, Dóm tér 7. H-6720 Szeged, Hungary
[b] MTA-SZTE Bioinorganic Chemistry Research Group, University of Szeged, Dóm tér 7. H-6720 Szeged, Hungary
[c] Centro de Química e Bioquímica (CQB), Faculdade de Ciências, ULisboa, Campo Grande, Lisbon, Portugal
[d] Centro de Química Estrutural (CQE), Faculdade de Ciências, ULisboa, Campo Grande, Lisbon, Portugal
[e] Centro de Química Estrutural (CQE), Instituto Superior Técnico, ULisboa, Lisbon, Portugal
[f] Centro de Ciências e Tecnologias Nucleares (C2TN), Instituto Superior Técnico, ULisboa, Estrada Nacional 10, Bobadela, Loures, Portugal
[g] Centro de Investigação Interdisciplinar Egas Moniz (CiiEM), Quinta da Granja, Monte da Caparica, Portugal

ABSTRACT

Two recently published Ru(III) complexes bearing (N_2O_2) tetradentate bis(aminophenolate) ligands, formulated as [Ru(III)(*salan*)(PPh$_3$)Cl] (where *salan* is the tetradentate ligand 6,6'-(1S,2S)-cyclohexane-1,2-diylbis(azanediyl)bis(methylene)bis(3-methoxyphenol) in complex **1**, or 2,2'-(1S,2S)-cyclohexane-1,2-diylbis(azanediyl)bis(methylene)bis(4-methoxyphenol) in complex **2**, and PPh$_3$ is triphenylphosphane) were studied herein to outline their antitumor mode of action. Previously, it was found that they were very active against human ovarian and breast adenocarcinoma cells (on a 72 h challenge). In this work, the human cisplatin-sensitive ovarian adenocarcinoma line A2780 was used as the cell model for further studies at a 24 h challenge. Both complexes are active, their cytotoxicity being comparable to that of cisplatin in the same conditions.

As a possible target in the cell for their action, the interaction of **1** and **2** with DNA was assessed through displacement of well-established DNA fluorescent probes (ethidium bromide, EB, and 4',6-diamidino-2-phenylindole, DAPI) through steady-state and time-resolved fluorescence spectroscopy. The complete emission spectra were analysed globally for the binary DNA – probe and ternary DNA – probe – Ru(III) complex systems. Both Ru(III) complexes can displace EB and bind to DNA with similar and moderate strong affinity with conditional stability constants of log K' = (5.05 ± 0.01) for **1** and log K'= (4.79 ± 0.01) for **2**. The analysis of time-domain fluorescence intensity decays confirmed both qualitatively and quantitatively the model used to describe the binding and competition processes. Cell studies indicated that apoptosis is the major mechanism of cell death for both complexes, with **2** (the more active complex) promoting that process more efficiently than **1**. Transmission electron micrographs revealed clear alterations on intracellular organization consistent with the induction of programmed cell death processes.

1. Introduction

Cancer is the second largest cause of death in developed countries. Recent statistics (2007-2009) indicate that two in every five people born today will be diagnosed with cancer at some time during their life.[1] According to the World Health Organization, cancer mortality is projected to rise to over 13.1 million people in 2030.[2]

Rosenberg's breakthrough of the antitumor activity of cisplatin in the sixties paved the way for the research and development of metal-based drugs in cancer chemotherapy.[3] Notwithstanding the remarkable advances in the field, three platinum-based compounds (cisplatin, carboplatin and oxaliplatin) remain to date the only approved metallodrugs for worldwide use in the chemotherapy of cancer given their outstanding efficiency.[4] However, numerous severe side-effects, their limited spectra of action and tumour resistance to treatment, either intrinsic or acquired during cycles of therapy, limit their clinical value. New and efficient alternative therapies are urgently and intensely sought for.

Ruthenium complexes have consistently shown excellent anti-cancer properties both *in vitro* and *in vivo*, and are quite promising as effective alternatives to platinum-based agents, typically offering a wider spectrum of activity and the potential to overcome platinum-resistance, as well as different mechanisms of action and, in general, lower toxicity.[5-7] The intense research on this field in the last few years has led to the development of several families of compounds, with a significant number of Ru(II) and Ru(III) complexes showing antitumor activity in a variety of cancer cell lines (including cisplatin resistant cells), ranging from inorganic-based agents to organometallic complexes.[5,8-11] Two Ru(III) lead compounds (NKP-1339 and NAMI-A) have indeed progressed successfully through phase I and preliminary phase II clinical trials in patients.[5,6]

The biological targets of antitumor ruthenium complexes have not been unequivocally identified and remain the subject of intense research. Serum protein binding is crucial for the *in vivo* behavior of drugs in general and in that of ruthenium-based agents in particular, since albumin and transferrin have been proposed to play a role in their mechanism of action. [8,9,12,13] It is proposed that albumin is involved in the transport of ruthenium compounds in the blood stream and can act as a Ru-compound warehouse[8,13]. Transferrin has been considered to play an important role in the cellular accumulation of ruthenium complexes (Ru(III) in particular) *via* transferrin-receptor mediated endocytosis.[8,13]

The set of co-ligands around the metal centre is in fact crucial in modulating biological behaviour of the overall complex in what concerns the cytotoxic activity, protein binding, subcellular distribution

and the interaction with DNA.[8,9,13] DNA is a classical target for metallodrugs in general. Although it may not be their primary target, it is very often involved in their mode of action.[6,7] Irreversible modifications in the control of cell division resulting in unrestrained cell proliferation are one of the hallmarks of cancer. The first genetic alterations identified in cancer cells were seen in master genes responsible for cell cycle regulation that resulted in high proliferation rate and resistance to apoptosis.[14] Thus, a highly desirable feature for a drug candidate is the ability to promote cell death in a controlled process such as apoptosis.

Although Ru(III) complexes NKP-1339 and NAMI-A undergoing clinical development show remarkable potential as anticancer drugs despite their low half-life in aqueous media, chemical stability is a common requirement for a successful pharmaceutical which it can be achieved by increasing the denticity of the ligand(s). Tetradentate N_2O_2 ligands combining phenolate oxygen hard donnors suitable for stabilizing ruthenium in the +3 oxidation state with strong nitrogen donors in chelating positions are quite attractive in this context.

We recently reported our first work on two new ruthenium octahedral complexes with the (N_2O_2) binding motif in tetradentate bis(aminophenolate) ligands (also known as 'salan'-type). These new Ru(III)-salan complexes were the first compounds of this type reported in the literature for antitumour purposes.[15] Both salan ligands **L1** ((6,6'-(1S,2S)-cyclohexane-1,2-diylbis(azanediyl) bis(methylene) bis(3-methoxyphenol) and **L2** (2,2'-(1S,2S)-cyclohexane-1,2-diylbis(azanediyl)bis(methylene)bis(4-methoxyphenol)) and their Ru(III) complexes formulated as [Ru(III)(L)(PPh₃)Cl] (see **Scheme 1**) were evaluated in several human tumor cell lines.

All compounds exhibited an antiproliferative effect to different extent depending on the line tested, and coordination of **L1** and of **L2** to the Ru(III) metal center resulted in enhanced activity in all cell lines.[15] Despite the structural resemblance of these ligands (the only difference being the *para-* or *meta*-position of the methoxy group relative to the O donor on phenolate rings) complexes **1** and **2** exhibited a somehow different profile in what concerned their activity: although similar and comparable to cisplatin against A2780 cells (cisplatin sensitive ovarian adenocarcinoma), in breast adenocarcinoma (MCF7 and MDAMB231) cells complex **2** was clearly more active than **1**, both compounds being more active than cisplatin against the MCF7 ERα+ (non-invasive) breast adenocarcinoma line.[15]

The role of serum proteins on the action of these complexes was assessed as well. Binding of both compounds to human serum albumin was strong enough to infer that their transport in the blood plasma by this protein is quite likely, although it was observed that **2** interacted with albumin more strongly than **1**.[15] Prior incubation of Ru(III)-salan complexes with albumin or transferrin seemed to

deactivate **2** to some extent in A2780 cells, the activity of **1** being fairly unaffected by the formation of the (protein-complex) adduct(s). Our results thus indicated that transferrin is likely to play a minor role (if any) in the uptake of these Ru(III) agents, and that alternative pathways should be proposed when clarifying their mode of action.[15] These differences in their behaviour stimulated our interest on understanding whether this structure-activity relationship would transpose into their pharmacological properties.
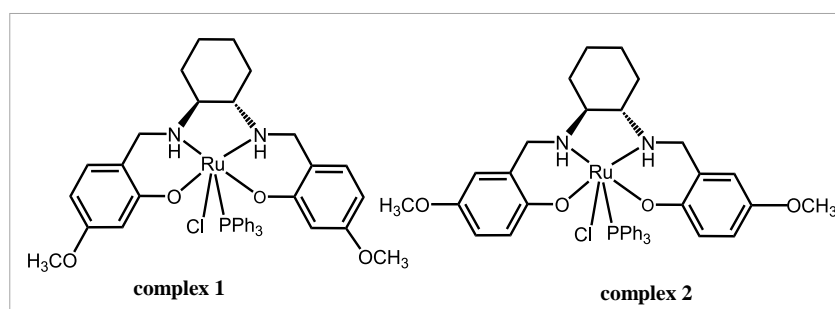
Scheme 1. Structures of the two [Ru(III)(*salan*)(PPh$_3$)Cl] complexes used in this study (PPh$_3$ is triphenylphosphane, P(C$_6$H$_5$)$_3$). *Salan* ligands **L1** and **L2**, and their corresponding [Ru(III)(L)(PPh$_3$)Cl] complexes **1** and **2** were synthesized as previously reported.[15]

In this work, we proceeded with further tests for the two Ru(III)-salan complexes and used the A2780 line as the cell model to clarify mechanisms behind their biological activity and to understand whether the small structural difference would transpose into their pharmacological properties, and with what impact. In particular, we focused on the role of DNA as a possible target, assessing this interaction through a novel quantitative approach to DNA-[metal complex] binding. We also evaluated the contribution of programmed cell death for their cytotoxicity, as well as their effect on the cell cycle of tumour cells and on the cell ultra-structural morphology.

2. Results and discussion

2.1. Interaction with DNA

2.1.1. Steady-state spectrofluorometric measurements

Fluorescent DNA probes ethidium bromide (EB) and 4',6-diamidino-2-phenylindole (DAPI) were used to characterize the interaction of the two Ru(III)-salan complexes (**Scheme 1**) with calf thymus DNA (ctDNA or DNA) since they exhibit negligible fluorescence at pH 7.4 in 10 mM 4-(2-hydroxyethyl)-1-piperazineethanesulfonic acid (HEPES)/2% (v/v) DMSO medium, and the interaction between ctDNA and either of the two Ru-salan complexes does not lead to any measurable fluorescence. Probe

1   displacement experiments are in fact ternary systems (consisting of the probe, DNA and the ruthenium

2   complex), and the binary systems (probe and DNA) must first be characterized in the experimental

3   conditions used.

4   EB and DAPI (**Scheme S1** in **Supporting Information**) have weak intrinsic fluorescence emission at

5   the appropriate excitation wavelengths, and the binding of these probes to DNA induces an increase of

6   fluorescence quantum yield. EB is known as an intercalative agent while DAPI is a minor groove

7   binder of DNA.[16,17] Adduct formation of both probes with DNA enhances the fluorescence intensity

8   (I_F) up to 44- and 15-fold for DAPI and EB, respectively (**Fig. 1**). At the same time a blue shift of the

9   emission can be observed (15 nm and 7 nm for DAPI and EB, respectively) due to the insertion of the

10   probe into a less polar environment as compared to the aqueous medium surrounding the unbound free

11   molecule.[18]

12

13
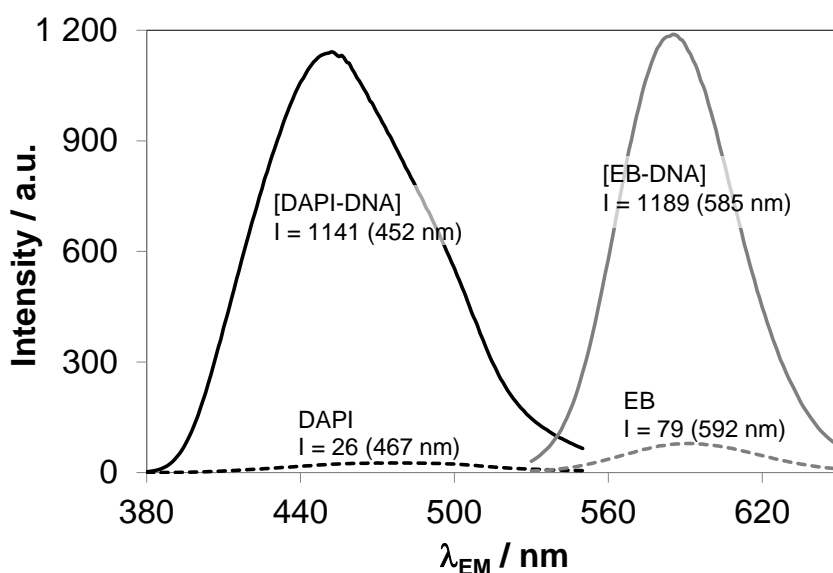
Fig. 1. Fluorescence emission spectra of DAPI (black dotted line), DAPI-ctDNA (black solid line), EB (grey

dotted line) and EB-ctDNA (grey solid lines). (C_{DAPI} = 3 μM; C_{EB} = 5 μM; λ_{EX} = 365 nm (DAPI) or 510 nm

(EB); [probe-DNA] spectra were obtained by probe-DNA titrations when the saturation of the probe with DNA

was achieved, $c_{ct\text{-}DNA}$ = 51 μM (DAPI), 15 μM (EB); t = 25 °C; pH = 7.40 10 mM HEPES/ 2% (v/v) DMSO).

18

19   Prior to the probe displacement experiments, the probe-DNA binding constants and the size of the

20   binding site were calculated on the basis of independent measurements. In order to evaluate the

21   binding site size of a probe on DNA two series of experiments are needed: measurements at constant

22   DNA concentration with varying probe concentrations and *vice versa*, where in both cases saturation

23   should be attained. Two "virtual" molar intensities (I_{molar}) can be calculated from the measured

24   intensities (corrected by the emission intensity of non-bound probe). The ratio of these values (I_{molar}(at

25   constant DNA concentration) / I_{molar}(at constant probe concentration)) gives an estimation of the

26   average binding site size represented in the number of the nucleotides (nuc).

1   To calculate the binding constants between DNA and the probes, complex formation between the

2   binding site of DNA and the probe is assumed to be a one-step reaction; hence it can be characterized

3   by one conditional binding constant (log K') (see details in **Supporting Information, Section S1**).

4   The binding constants were calculated with the computer program PSEQUAD.[19] The PSEQUAD

5   program was originally developed for determination of stability/binding constants from experimental

6   equilibrium data collected by various methods such as pH-potentiometry, and/or spectroscopy

7   (UV/Vis, NMR), and this software can also be used on fluorometric data evaluation as reported

8   previously for protein-ligand (metal complex) interactions.[20,21] After a set of iterative steps, the

9   program provides the binding constants of the selected adducts with standard deviations and the molar

10   emission spectra of the emitting components/adducts. Calculations were performed for different sizes

11   of the binding site (*i.e.* different number of nucleotides), and the best fit for EB and DAPI was found

12   for 5 and 23 nucleotides, respectively. In **Fig. 2** the measured and calculated fluorescence intensities

13   are shown for the EB – DNA system considering binding site sizes of 4, 5 and 6 nucleotides, as well as

14   the experimental data. The calculated values (average binding site size) were based on the results of

15   PSEQUAD calculations, namely the binding constant and molar intensities. Although the fit for any of

16   the assumed binding site sizes seems to be very similar at a first glance, a deeper statistical analysis

17   revealed that the best fit is obtained for an average binding site size of 5, which is in good agreement

18   with literature data[16,22,23] and the log K' value obtained is collected in **Table 1**. Further refinements did

19   not result in any appreciable improvements in fitting to the experimental data.
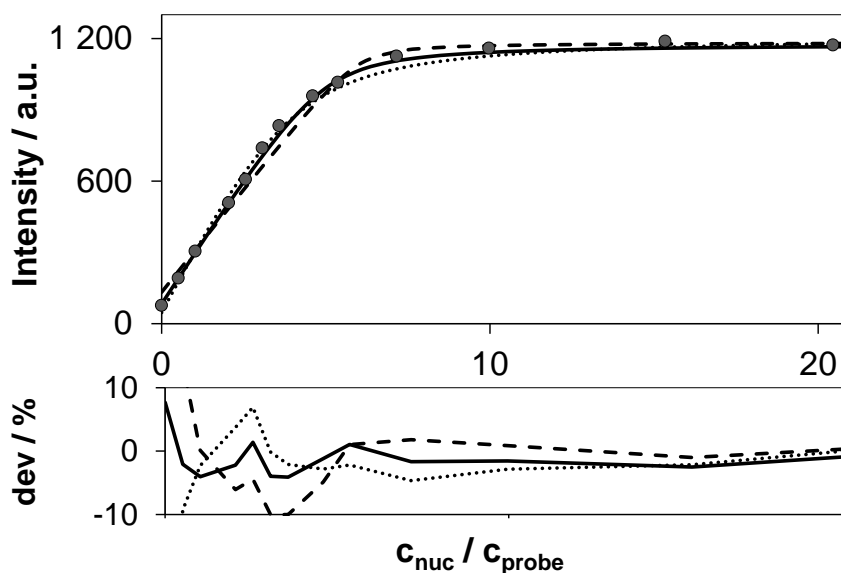
20

21   **Fig. 2.** Total fluorescence intensity of EB samples titrated by ctDNA: *up*: measured data (●) and simulated

22   curves for binding site sizes n = 4 (dotted line), 5 (black line) or 6 (dashed line); *below:* deviation (dev.) of

23   simulated curves from measured intensities in %; ((c_{EB} = 5 μM; c_{nuc} = 0-100 μM; λ_{EX} = 510 nm; λ_{EM} = 585 nm;

24   *t* = 25 °C; pH = 7.40 (10 mM HEPES/2% (v/v) DMSO); simulated values based on PSEQUAD calculations –
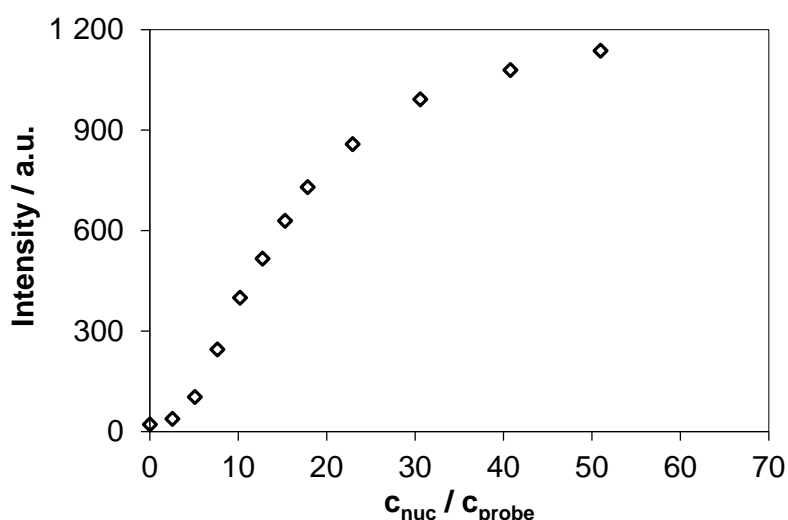
25   see **Table 1**).

26

Table 1

The interaction of DAPI with DNA is much more complicated, the binding mode presumably varying with the increasing ratio of DAPI-to-nucleotides. The appearance of a sigmoidal shape in the measured fluorescence emission intensity (**Fig. 3.**) confirms the existence of at least two different binding modes of DAPI to DNA that has an effect on the quantum yield of the DNA-DAPI adduct. Other works based on various techniques reported the existence of two distinct DNA-DAPI adducts depending on the molar ratio.[17,24,25] This behaviour is also observed for samples where the DNA concentration was kept constant and DAPI concentrations were varied (**Fig. 4.** and **Fig. S2**.). Normalized spectra undoubtedly show a significant red shift of the emission maxima at 1:2 and 1:5.6 DAPI-to-DNA ratios compared with the spectrum of DAPI without DNA (**Fig. 4**.). This effect is usually explained by the intercalative interaction between DNA and the probe.[17,25] The spectrum recorded at high excess of nucleotides (DAPI: nucleotide = 1:14) represents the expected typical blue shift associated with groove binding. Under these conditions, a binding site size of 23-26 nucleotides and a log K' value of (6.42 ± 0.22) could be estimated (**Table 1**). The nature of the interaction at higher DAPI/nucleotide ratios is however not relevant at the conditions used here for ternary systems.

Eriksson *et al.* published a value of 10 nucleotides (5 base pairs) for the interaction of DAPI with synthetic poly{d(A-T)2} DNA.[26] The difference between our findings and this data can be explained by the use of different DNA source, and reflects the base sequence within the nucleotide chain. DAPI prefers A-T rich sequences and ctDNA has roughly 40% G-C (42 mole % G-C, 58 mole % A-T). Hence, when using spectroscopic methods, the estimated value for the binding site size also expresses the frequency of the preferred base sequence within the nucleotide chain.

1
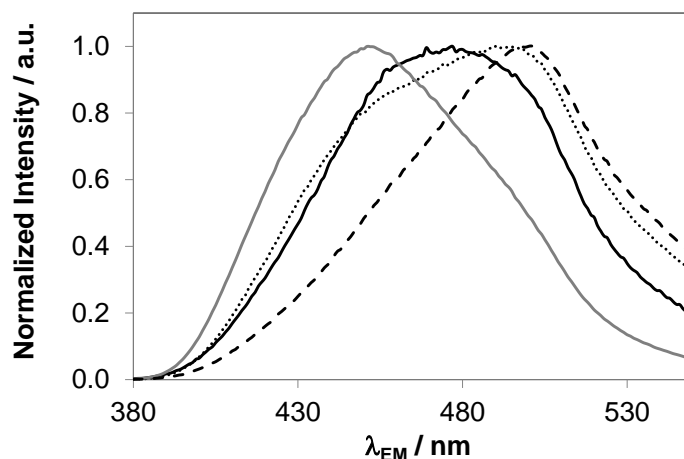
2

3 **Fig. 4.** Normalized emission spectra for the DAPI-DNA system at various DAPI:nucleotide ratios: 1:0 (black

4 line), 1:2 (dashed line), 1:5.6 (dotted line), 1:14 (grey line); {c_{DAPI} = 0.5-13 μM; c_{nuc} = 26 μM; λ_{EX} = 365 nm; t =

5 25 °C; pH = 7.40 (10 mM HEPES/ 2 % (v/v) DMSO)}.

6

7 An important factor to consider when comparing literature data, in addition to the specific

8 experimental conditions, is the calculation method used. Binding constants found in the literature are

9 typically obtained by graphical methods such as Lineweaver-Burk, Stern-Volmer or Hildebrand-

10 Benesi (the former two approaches are used for fluorometry data, the latter one for UV-Vis

11 measurements), and are not directly comparable with our results since the methods mentioned do not

12 take into consideration the actual size of the binding site.[18,27-29] These approaches are somewhat

13 limited since the analytical (total) concentration of DNA and probe are used instead of their

14 equilibrium (free) concentrations, and only one emitting species is usually proposed. They should be in

15 most cases considered as an empirical description of the results allowing only for comparison of the

16 binding affinities of different compounds measured under the same experimental settings.[30] The use of

17 analytical instead of equilibrium concentrations leads to only a rough estimate of the binding constants

18 (see **SI** for details). It is also noteworthy that authors often do not mention whether the binding

19 constants are calculated on the basis of the concentration of DNA in nucleotides or in base pairs,

20 which results in different values that again are not comparable with each other. Our approach using

21 PSEQUAD circumvents these limitations by calculating the binding constant(s) involved from actual

22 equilibrium concentrations of all species present in each system, as well as the binding site size (in

23 probe-DNA binary systems) and the stoichiometry of the adduct(s) formed, affording a more reliable

24 quantitative evaluation of the systems being studied.

25 Considering the ternary systems, probe displacement reactions with both Ru(III) complexes were

26 carried out using constant DNA and probe concentrations, and varying the concentration of the metal

27 complex. The ratio of DNA-to-EB was chosen as 1:4, and at this EB excess we could calculate that

28 83% of the probe is bound to DNA. **Fig. 5A** shows the effect of complex **1** and **2** on the emission

1 intensity measured for the DNA-EB adduct. The simulated curves are in good agreement with the

2 experimental data (see **Fig. S3**). This suggests that the complex can displace the intercalated EB from

3 its binding site with a concomitant decrease in the measured intensities, however the formation of a

4 ternary DNA adduct containing both the probe and the bound metal complex is also feasible. The fact

5 that no shift of the emission maximum is observed together with the results from our time resolved

6 experiments (*vide infra*) confirms the simple displacement hypothesis. The binding constants

7 calculated for the complexes (**Table 1**) is only valid for EB "binding sites" since the size of binding

8 site (or binding frequency) of complex **1** and **2** on DNA is most likely not the same as in the case of

9 EB. In order to solve this question, it would be helpful to see the saturation section of the displacement

10 reaction, which was not attainable due to solubility limitations at higher concentrations.

11 A similar behaviour was found for both complexes in the displacement reactions with EB, although the

12 estimated binding constant was somewhat lower for complex **2** (see **Table 1**).

13 To assess the possible interactions of the metal complexes and DNA at its minor groove, DAPI was

14 used at fixed DAPI:DNA ratio of 1:25 and the fluorescence emission intensity recorded is depicted in

15 **Fig. 5B**. In this case, even for a 12-fold excess of metal complex **1** or **2** the extent of quenching is only

16 *ca.* 10%, *i.e.*, no remarkable changes in the measured emission intensities were observed (see **Fig S4**

17 for fitted curve). The probe-DNA displacement reaction for both complexes is less extensive in the

18 case of DAPI as compared to EB, and thus our results suggest that binding at the minor groove is not

19 the preferred mode of interaction with ctDNA for the two Ru(III) complexes studied.

20
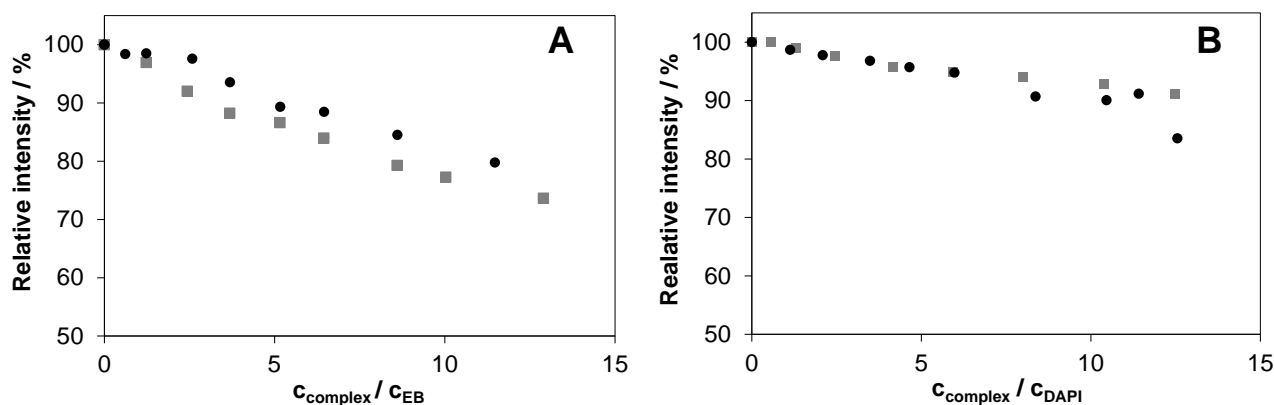
21
22

23 **Fig. 5.** Relative fluorescence intensity measured for the EB – DNA (A) and DAPI – DNA (B) system titrated by

24 complexes **1** (■) and **2** (●) {c_{EB} = 5.0 μM; c_{DAPI} = 3.1 μM; c_{nuc} = 19.2 μM (A) or 77.1 μM (B); λ_{EX} = 510 (A),

25 365 (B) nm; λ_{EM} = 595 (A), 450 (B) nm; t = 25 °C; pH = 7.40 (10 mM mM HEPES)/ 2 (v/v) % DMSO)}.

26

27 *2.1.2. Time-resolved fluorescence measurements*

28

29 Fluorescence lifetime measurements were carried out in order to have a deeper insight into the nature

30 of the interaction of the metal complexes **1** and **2** with DNA. The lifetime of the probe alone (EB and

9

DAPI) and of probe-DNA adducts (EB-DNA and DAPI-DNA) were obtained in independent experiments prior to the competition studies. The fluorescence intensity decays of free EB (assessed using samples without DNA) were very well described by a single exponential, with an associated lifetime of 1.8 ns (**Fig. 6**). In the case of the samples containing EB and DNA, the intensity decay was always described by a sum of two exponentials because there was always a fraction of free probe in solution. Indeed, the fluorescence lifetime of one component of the exponential fit was similar to that obtained in the absence of DNA (1.86 ns), and the other one was 21.2 ns (**Table 2**). Both these values are in very good agreement with literature data for free and DNA-bound EB, respectively. The large difference between these two lifetime values allows to separate very easily the contributions of DNA-bound and unbound EB to the total fluorescence decay in a sample where both species are present. Moreover, it is consistent with the marked increase in fluorescence intensity previously described for the emission spectra of the probe (**Fig. 1**).

In the EB-DNA system (**Fig. 6**) the fluorescence intensity decay is very well described as a sum of two exponentials in both the presence or absence of the studied metal complexes (**Table 2**), indicating the presence of only two emitting species in the system. Additionally, the lifetime retrieved for the adduct [EB-DNA] is not significantly changed at a 13-fold excess of the metal complexes, which can exclude the possibility of collisional quenching, or any other mechanism of interaction where *e.g.* both probe and metal complex would be interacting at the same DNA site. The same fluorescence lifetime values for the free and for the bound probe are retrieved in the ternary systems, which indicates not only the presence of only two emitting species in solution, but also that these are the same species as in the probe – DNA binary systems. This shows that the reaction taking place in solution is a true displacement reaction and that neither of the Ru(III) complexes are damaging the DNA structure, thus preventing EB from binding in the same way as in the absence of the compounds. In **Table 2**, results for EB – DNA system in the presence of increasing amounts of complex **1** and **2** are shown.
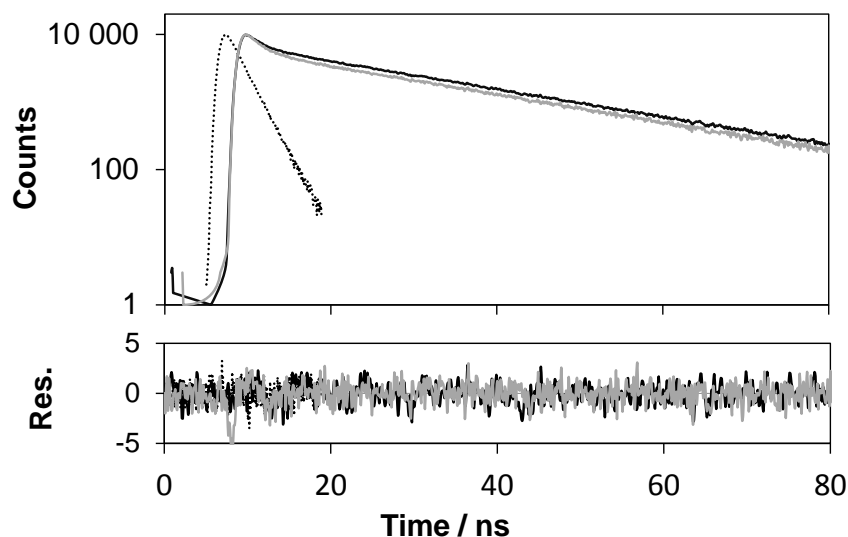
Fig. 6. Intensity decay of the emission fluorescence of EB alone (black dotted line), of EB – DNA (black line), and of EB – DNA – (complex **2**) (grey line) systems {c_{EB} = 5.0 µM; c_{nuc} = 19.5 µM; $c_{complex\ 2}$ = 63.9 µM; λ_{EX} = 460 nm; λ_{EM} = 590 nm; t = 25 °C; pH = 7.40 (10 mM HEPES/2% DMSO)} and (bottom) residuals plot for the fitting of each decay in the ternary systems with a sum of two exponentials (τ_1 = 1.86 ns, τ_2 = 21.2 ns – see **Table 2**).

Time-resolved fluorescence is a sensitive enough technique to differentiate the contribution from two emissive species even when one of them is a minor contributor to the overall fluorescent signal. In this way, if the changes in average fluorescence lifetime calculated from the two-exponential fit to the fluorescence intensity decay of EB are in quantitative agreement with the binding model proposed with log K' values calculated with PSEQUAD (*vide supra*), it further supports the suitability of the model.

Table 2

The pre-exponential of the short lifetime component (α_1) increases as the concentration of Ru(III) complex is increased (for both **1** and **2**), which is the expected trend for an EB displacement from DNA. The fraction of light emitted by free probe (f_1) is always below 11%, but it is still possible to appreciate its increase upon complex addition to the system, highlighting the fact that it is possible to separate the contribution from both species using time-resolved fluorometry. Moreover, it justifies the trend observed for the steady-state fluorescence intensity decrease observed in the competition experiment with EB (**Fig. 5**) where the extent of quenching never attained even 50%. This does not mean that the compound under test has a weak interaction with DNA, but reflects merely the fact that even a very small fraction of DNA bound probe will contribute a very significant fraction of light to total emission.[31] The amplitude-averaged mean fluorescence lifetime (τ_{av}) is a measure of the

11

fluorescence quantum yield in the absence of static quenching. It decreases by 22% for a complex **1**: EB ratio of 1:12.0. This is in excellent agreement with the simulated curve based on PSEQUAD calculations shown in **Fig. S3**. Such result not only rules out that a static quenching process could occur, *e.g.* by an interaction of probe with the complex in solution, but also it quantitatively validates the binding model proposed (**Table 1**). For complex **2**, τ_{av} decreases by 15% for a complex: EB ratio of 10.5, which is also in agreement with the binding constant present in **Table 1**.

Similar measurements were performed with DAPI. Again, a single exponential function yielded a good fit to the experimental intensity decay for the probe in solution (without any improvement by adding further exponentials). The value retrieved for the fluorescence lifetime of DAPI (in the absence of DNA) was 1.57 ns, in close agreement with the literature.[18] The fluorescence intensity decay of DAPI was also measured in the presence of DNA and complexes **1** and **2** (**Table 2**). As for EB, the fluorescence decay became a bi-exponential function, with one component coincident with the one observed for free DAPI, and a longer component of 3.6 ns assigned to DNA-bound probe. In contrast to the observations with EB but in agreement with the steady-state intensity results (**Fig. 5B**), the average fluorescence lifetime for DAPI and the adduct [DAPI-DNA] are barely changed upon addition of metal complexes. Noteworthy is the fact that although the noted changes are rather small for both complex **1** and **2**, it is slightly stronger for the latter, a behaviour also suggested by the fluorescence intensity results of **Fig. 5B**. This might denote that this compound may have a very mild minor groove binding ability, or because it is not such a strong intercalating agent as **1** it may be more available for non-specific interactions with DNA eventually displacing a small fraction of the minor groove binder DAPI.

To summarize, the interaction of both Ru(III)-salan complexes with DNA is assessed by steady-state and time-resolved fluorescence spectroscopy using the probes EB and DAPI. In this work we use a method for evaluating fluorescence results that provides the conditional stability binding constants for the interaction by an iterative procedure based on the true equilibrium concentrations for all species present in solution, in contrast with other methods reported in the literature where total concentrations are used instead. Our approach also affords the binding site size involved in DNA-probe interactions without any *a priori* assumptions. Time-resolved fluorescence spectroscopy enabled to identify the emitting species in these systems. In both DNA–probe binary systems and DNA–probe–Ru(III) complex ternary systems, the only two fluorescent species observed are the bound and unbound probe, the concentration of the latter reflecting the increase in the concentration of the Ru(III) complex as a consequence of the competition reaction. EB is displaced from its DNA adduct in the presence of both Ru(III) complexes, and the competition experiments afford stability constants for the interaction of complexes **1** and **2** with DNA with higher accuracy than in the case of DAPI. It was possible to estimate stability constants from the effect of **1** and **2** on the displacement reaction of DAPI from the

1 DNA-DAPI adduct, which yielded the same value for both complexes but since the effect observed in

2 these systems is quite small, these $K'_{binding}$ values must be taken as rough estimates. Log $K'_{binding}$ values

3 obtained indicate that the interaction is moderately strong, and suggest that the interaction of **1** with

4 DNA is somewhat stronger than that of **2**.

5

6 These results are not reflecting the relative cytotoxic activity (IC_{50} values) observed for these

7 complexes, with **2** being more active than **1** in all cell studies done (at either 24 h or 72 h challenges).

8 As such, DNA is a possible molecular target for these complexes, but other targets are most probably

9 involved in their action as well.

10

11 ***2.2. Studies with ovarian adenocarcinoma cells***

12

13 *2.2.1. Cytotoxic activity and mechanism of cell death*

14

15 The cytotoxic activity of complexes **1** and **2** was evaluated in human cisplatin sensitive ovarian

16 adenocarcinoma A2780 cells for a 24 h incubation to allow a suitable choice of the concentrations to

17 use in the flow cytometry assays which involved a 24 h incubation period. The IC_{50} values determined

18 in these conditions were 50 µM for complex **1** and 30 µM for complex **2**. These values are comparable

19 to the cytotoxic activity of cisplatin for A2780 cells in the same conditions (after a 24 h incubation

20 period), 36 µM (**Fig. 7A**), and the quantitative relation among the IC_{50} values for these compounds is

21 in general the same as observed for a 72 h challenge.[15]

22

23 The mechanism of cytotoxicity induced by complexes **1** and **2** was assessed by flow cytometry

24 analysis of cells stained for Annexin-V, a Ca(II)-dependent phospholipid-binding protein with high

25 affinity for phosphatidylserine (FL1), and propidium iodide (PI, that stains DNA of permeabilized

26 cells and shows unviable cells). Fluorescence of PI (FL3) was plotted versus Annexin-V fluorescence

27 (FL1) as shown in **Fig. 7B**.

28 Viable cells are both Annexin-V and PI negative (Annexin-V⁻/PI⁻), while cells that are entering

29 apoptosis are Annexin-V positive (Annexin-V⁺) and progressively more positive for PI. **Fig. 7B** shows

30 the majority of control cells stained negative for both PI and Annexin-V, corresponding to viable cells.

31 Cells treated with low doses of the compounds showed a small population of Annexin-V⁺ PI⁻ cells,

32 indicating apoptosis at an early stage. As expected, with higher complex concentrations, the population

33 of double positive cells increased indicating an increase in apoptosis. Taken together, results show that

34 both complexes **1** and **2** induce cell death mainly through an apoptotic process, and that complex **2**

35 promotes this more efficiently than **1**, an interpretation validated by the good correlation with the

36 cytotoxic activity data (**Scheme 1** and **Fig. 7A**).[15]

A

B Control

Complex 1, 30 µM   Complex 1, 50 µM   Complex 1, 70 µM

Complex 2, 10 µM   Complex 2, 30 µM   Complex 2, 50 µM
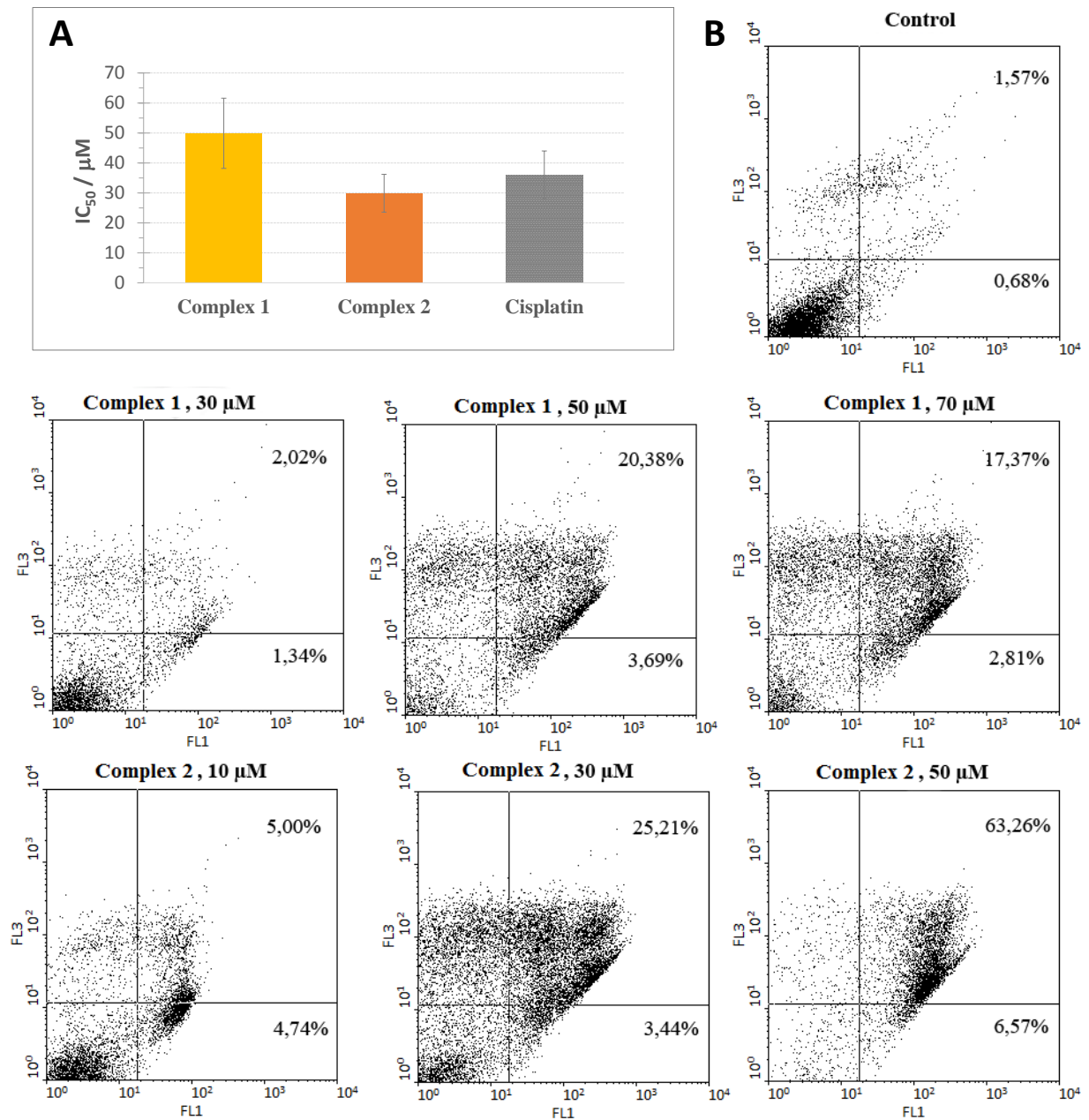
Fig. 7. Effect of complexes **1** and **2** in A2780 cells in a 24 h challenge: A) Cytotoxic activity (measured as the IC_{50}) for both complexes and for cisplatin tested in the same conditions, and B) Quantification of apoptosis in cells treated with complexes **1** and **2** using the Annexin-V/PI double staining assay. A2780 cells (control) were treated with 30, 50 and 70 µM of complex **1** and 10, 30 and 50 µM of complex **2** for 24 h, and stained with FITC-conjugated Annexin-V and PI. Fluorescence was analyzed by flow cytometry. The dual parametric dot plots combining Annexin-V (FL1) and PI (FL3) fluorescence show the viable cell population in the lower left quadrant Annexin-V$^-$/PI$^-$, the early apoptotic cells in the lower right quadrant Annexin-V$^+$/PI$^-$, and the late apoptotic cells in the upper right quadrant Annexin-V$^+$/PI$^+$. Data shown are a representative experiment of two independent experiments with similar findings.

2.2.2 Effect of Ru(III)-salan complexes on the cell cycle

To investigate whether **1** and **2** affect cell cycle progression, cell cycle analysis was assessed by flow cytometry in A2780 cells treated with the Ru(III) complexes for 24 h at the IC_{50} concentration. **Fig. 8** shows that the effect of complexes **1** and **2** in the cell cycle of A2780 cells is different. While control cells were mainly in G1/G0 and G2/M phases of cell cycle (**Fig. 8A**), the cycle progression was altered after treatment with complex **1** (**C1**), leading to a decrease in the percentage of cells in the G1/G0 phases and an increase in the proportion of cells in the S phase of the cell cycle compared to the control (**Fig.8B**). This result suggests that complex **1** might induce cell cycle arrest at G2 or M phases indicating that it might induce incomplete DNA synthesis (G2 checkpoint) and/or disruption of the mitosis process including alterations in the chromosome assembly and/or in the spindle formation (**Fig. 8D**). These alterations are not repaired by cellular mechanisms resulting in apoptosis. By contrast, cells treated with complex **2** (or **C2**) presented a decrease in the percentage of cells in S and G2/M phases of the cell cycle compared to control (**Fig. 8C**), which suggests that complex **2** efficiently induces apoptosis with a minor effect on cell cycle arrest, and that **2** might induce DNA damage or dysfunctional metabolic state that prevents cell cycle progression to the synthesis phase (S).

The dissimilar effect observed on the A2780 cell cycle promoted by these complexes could be related to the different importance that DNA has as a molecular target for each compound (**Table 1, Fig. 6**). In fact, although both complexes could efficiently displace EB from ctDNA, the one that was able to do it more efficiently is the compound with higher IC_{50}, suggesting that other cellular targets contribute to the cytotoxic activity. The different position of the methoxy group in the benzene ring may influence the hydrophilicity of the compound. In fact, complex **2** has a more hydrophilic character than complex **1** (see **Supporting Information**, **Section S2**), which might influence their relative affinity for different sub-cellular structures, *e.g.* cellular membranes or cytoskeleton.
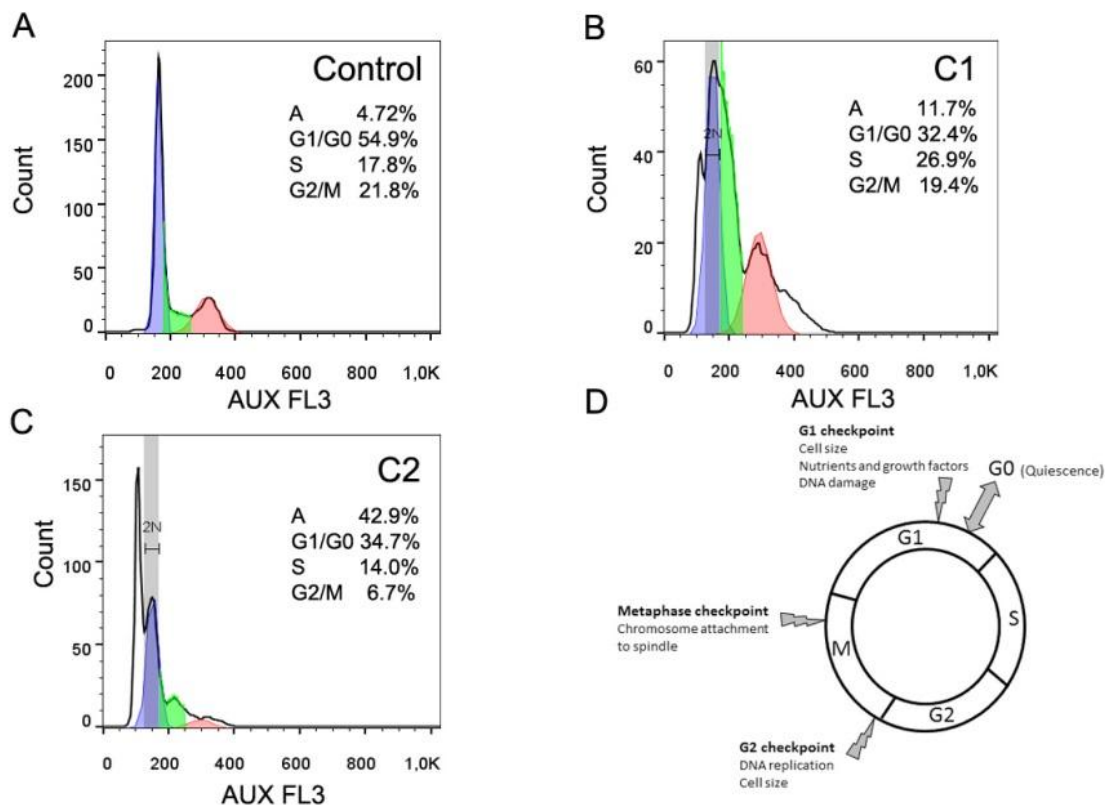
Fig. 8. Cell cycle analysis of A2780 cells in control (**A**, cells with no treatment), treated with complex **1** (C1) (**B**) and treated with complex **2** (C2) (**C**), and schematic overview of cell cycle regulation including the cell cycle checkpoints (**D**). Cells were treated with the complexes (30 μM for **1,** 10 μM for **2**) for 24 h and were analyzed by flow cytometry; values indicated are the percentage of cells in the different phases of the cell cycle; *insets -* A: apoptosis; G1/G0: Gap 1 and Gap 0 S: DNA synthesis G2: Gap 2; M: mitosis.

2.2.3. Ultrastructural analysis and effect on cell morphology

Transmission Electron Microscopy (TEM) was used to investigate the effects of both ruthenium complexes on the morphology of ovarian cancer cells. The ultrastructure analysis by TEM can give an indication of the cell damage brought upon by the action of prospective anticancer agents. By affording ultra-resolution images, it allows detecting morphological changes associated with the action of the agents being tested, points out potential intracellular targets, and makes apparent alterations in cell physiology, thus providing information on the underlying mechanisms of action and potential targets in the cell. Both complexes **1** and **2** were analyzed for their effect on A2780 cells after a 24 h incubation period, and images of treated and untreated cells were compared. **Fig. 9** depicts representative TEM images recorded in each case.

16

As can be seen in **Fig. 9B**, cells treated with complex **1** exhibit an underdeveloped/shrunken Golgi apparatus and the lysosomes present a heterogeneous content. Golgi fragmentation is recognized as an early apoptotic event.[32] Although mitochondria seemed normal, breaches in the cytoplasm could be observed suggesting disorganized membranes. These observations are in contrast with those of controls (**Fig. 9A**) confirming the effects of complex **1** on the endomembrane system. Cells treated with complex **2** (**Fig. 9C**) show enlarged lysosomes, but most noticeably, large vacuolar structure, with the prototypical morphology of autophagic vacuoles, suggesting that (macro)autophagy might be occurring. Annealed nucleoli were also observed, suggesting that complex **2** induces the inhibition of ribosome synthesis, may be as a result of DNA dysfunction. Overall, cell alterations are more marked with compound **2** that display signs of profound and probably irreversible cellular damage. This could be consistent with increased late apoptosis induced by compound **2** found by flow cytometry. However, until recently apoptotic cell death and autophagy (that could also lead to cell death) have been considered in general mutually exclusively processes. Nonetheless, it is currently known that in certain cases, a mixed apoptotic-autophagic route can be followed as a different type of programmed cell death.[33] Therefore, it is tempting to speculate that compound **2** could be inducing this sort of process, a hypothesis that we will test with more detailed studies on the cell death mechanism induced by complex **2** in the near future.
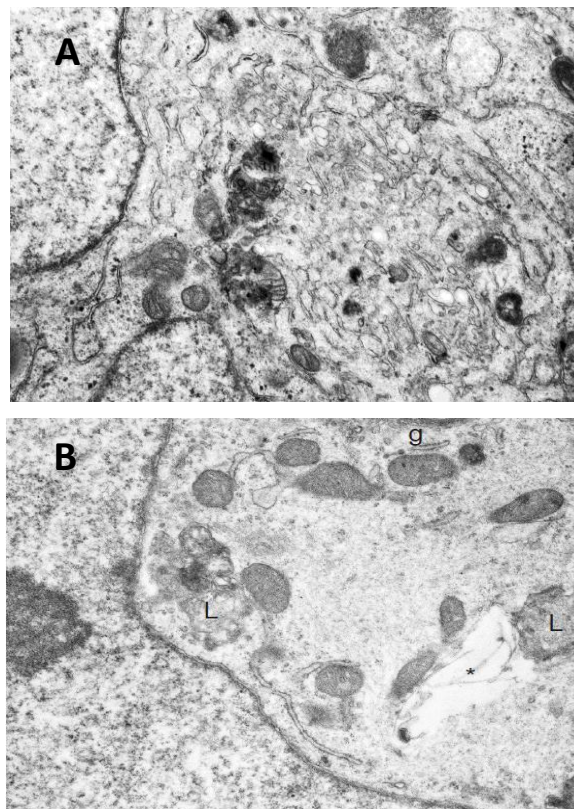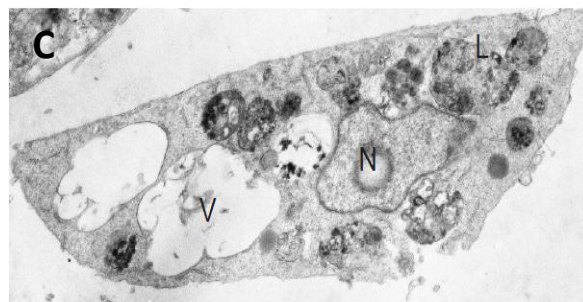
Fig. 9. Representative TEM images showing the morphology and ultrastructure of A2780 cells (g - Golgi apparatus; L - lysosomes; N – nucleolus; V- vacuoles). (**A**) Controls (untreated cells) showing normal well developed Golgi apparatus; (**B**) cells treated with complex **1** (50 μM, 24h) showing underdeveloped Golgi System; Lysosomes with heterogeneous content, and breaches in the cytoplasm suggesting disorganized membranes; (**C**) cells after treatment with complex **2** (50 μM, 24h) showing annealed nucleolus indicating the inhibition of ribosome synthesis, large lysosomes suggesting autophagy and large vacuoles.

3. Conclusions

Two Ru(III)-salan complexes with promising antitumor activity were evaluated to outline the basis of their biological action. DNA, typically involved in the mode of action of metallodrugs, is usually proposed as a possible target and the interaction of both complexes with the biopolymer was assessed by steady-state and time-resolved fluorescence spectroscopy using competition experiments with the well-established probes EB and DAPI. Although the displacement effect from its DNA adduct observed with DAPI in the presence of both Ru(III) complexes is quite small, EB displacement afforded accurate stability conditional binding constants for **1** and **2**. Log K'$_{binding}$ values obtained indicate that the interaction is moderately strong, and suggest that the interaction of **1** with DNA is somewhat stronger than that of **2**. These findings indicate that DNA is a possible molecular target for these complexes, but other targets are most likely involved in their mode of action. In fact, this data is not reflecting the relative cytotoxic activity observed, with **2** being more active than **1** in all cell studies done, and results on the morphology and cycle progression of A2780 cells treated with the two compounds seem to support this hypothesis.

In what concerns the mechanism of cell death, both complexes were found to induce apoptosis in A2780 cells with complex **2** being the most efficient. This finding is in agreement with the cytotoxic activity found for the complexes considering apoptosis as the main cell death mechanism.

In the cell cycle of A2780 cells complex **2** induces apoptosis without a relevant effect of cell cycle arrest. This suggests that **2** might induce DNA damage or a dysfunctional metabolic state that precludes cell cycle progression to the synthesis phase, which is in agreement with the autophagic

18

1   process suggested by the ultra-structural analysis observed in cells treated with **2**. In contrast, results

2   for complex **1** suggest that it may induce cell cycle arrest at G2 or M phases, resulting in promoting

3   apoptosis.

4   The distinct effect induced by these Ru(III) complexes on the A2780 cells is probably related to

5   differences in their hydrophilicity. In fact, complex **2** has a more hydrophilic character than **1**, which

6   indicates differences in how they interact with plasma and intracellular membranes *in vivo* are to be

7   expected, and would have an impact in their cellular uptake.

8   The fact that cell morphology is affected in a different manner upon incubation with **1** and **2** further

9   supports the hypothesis that several targets are involved in their action. This is in agreement with the

10   belief that Ru-based metallodrugs exert their effect through multiple targets.[13] This might be a valuable

11   advantage when compared with other anti-cancer agents, either by allowing the use of lower doses *in*

12   *vivo* (thus reducing side effects) or by rendering the development of chemoresistance by tumor cells

13   more difficult. The results presented in this work add further support for the high potential of these

14   Ru(III)-salan complexes as prospective metallodrugs for cancer therapy and highlights the striking

15   impact that small differences in the structure of the ligands coordinated to the metal centre may have

16   on the biological response of the overall compound.

17

18

19   **4. Materials and Methods**

20

21   *4.1. Chemicals*

22

23   Deoxyribonucleic acid sodium salt from calf thymus (ctDNA), ethidium bromide (EB), 4',6-

24   diamidino-2-phenylindole (DAPI), 4-(2-hydroxyethyl)-1-piperazineethanesulfonic acid (HEPES),

25   dimethylsulfoxide (DMSO) and ethanol were purchased from Sigma-Aldrich and used without further

26   purification. RPMI 1640 with L-Glutamine, Tripsin-EDTA, Penicilin/Streptomicin, phosphate buffer

27   saline (PBS) and fetal bovine serum (FBS) were purchased from Invitrogen. Propidium iodide (PI) and

28   Ribonuclease (RNase) were purchased from Sigma-Aldrich, and Annexin-V from BD Biosciences.

29   Complexes **1** and **2** were synthesized and characterized as previously reported.[15] Millipore® water was

30   used for the preparation of all aqueous solutions.

31

32   *4.2 Sample preparation for spectrofluorometric measurements*

33

34   Samples were prepared in 10 mM HEPES buffer (pH 7.40). Concentrated DNA stock solutions (*ca.* 1

35   mg/mL) were prepared by gently hydrating the solid DNA in pH 7.40 HEPES buffer, leaving it

36   overnight at 4 °C on an orbital stirrer with slow gentle shaking. DNA concentrations, expressed in

nucleotide units, were determined by UV spectrophotometry using the molar absorption coefficient 6600 $M^{-1}cm^{-1}$ at 260 nm.[38] The ratio of UV absorbance at 260 and 280 nm was checked for each new stock solution, and the ratio $A_{260nm}/A_{280nm} \geq 1.8$ indicating that the DNA was sufficiently free of proteins.[34] DNA stock solutions were stored at 4 °C and used within a maximum of 4 days. Stock solutions of EB and DAPI were prepared by dissolving a known amount of the probe in Millipore® water and were kept in dark for sample preparation.

Spectroscopic measurements were carried out on individually prepared samples to ensure the same pre-incubation time at (25±1)°C for all samples in each assay. Due to the limited solubility of complexes **1** and **2** in aqueous media, DMSO was used to prepare concentrated stock solutions of each complex, followed by appropriate dilution with DMSO (if needed) and 10 mM HEPES buffer (pH 7.40) to obtain the desired complex concentration and DMSO content, kept constant as 2% (v/v) in the final samples. Dilutions were carried out immediately prior to sample preparation. Data presented are the mean value ± standard deviation of at least 3 independent assays.

4.3. Steady-state spectrofluorometric measurements

Fluorescence measurements were carried out on a Spex Fluoro-log 3-22/Tau 3 spectrofluorometer equipped with double grating monochromators in both excitation and emission light paths from Horiba Jobin Yvon at room temperature. For measurements with the probes EB and DAPI at 25.0 ± 0.1 °C semi-micro quartz cells (1 cm × 0.41 cm) from Hellma were used. Samples usually contained 3-5 μM probe, and various probe:nucleotide ratios (from 1:0 to 1:50) were used. In the probe displacement experiments the probe-to-nucleotide ratio was 1:4 and 1:25 for EB and DAPI, respectively, and the concentrations of complexes **1** and **2** were varied at 0-64 μM after 60 min incubation in the dark. The excitation wavelengths were 510 nm for EB (with 4 nm/4 nm bandwidths for excitation and emission, respectively) and 365 nm for DAPI (2 nm/2 nm slit widths) and the fluorescence emission was measured in the range of 380-650 nm depending on the experiment. The conditional binding constants were calculated with the computer program PSEQUAD.[23] Data were also analysed by Lineweawer-Burk linearization method for comparison (see **Supporting Information**, **section S1**).[27]

Corrections for self-absorbance and inner filter effect were necessary in the steady-state fluorometric experiments since the emitted light is partly absorbed by the probes and by the Ru(III) complexes. Corrections were carried out according to the equation (1),

$$I_{corr} = I_{meas} \times 10^{(A_{EX}+A_{EM})/2} \quad (1)$$

where I_{corr} and I_{meas} are the corrected and measured fluorescence intensities, A_{EX} and A_{EM} are the absorbance values at the excitation and emission wavelengths in the samples, respectively.[18] The geometry of the cell was considered when executing the corrections. The spectrophotometric

1 absorption measurements were recorded on a Jasco V-560 (Tokyo, Japan) double beam
2 spectrophotometer.
3
4 *4.4. Time-resolved fluorescence measurements*
5
6 Fluorescence lifetime was measured using nanoLED N-460 for EB (λ_{EM} = 590 nm, 15 nm/ bandwidth)
7 and N-370 for DAPI (λ_{EM} = 450 nm, 2 nm bandwidth) light sources (Horiba Jobin Yvon) using time
8 correlated single-photon counting (TCSPC) mode. The resolution of the detection system was 50 ps.
9 The number of counts on the peak channel was 20000 (for DAPI samples) or 10000 (for EB samples).
10 The number of channels per curve used for the analysis was *ca.* 1000 for EB-DNA, *ca.* 400-600 for
11 DAPI and *ca.* 300 for EB alone, with a time scale of 0.05552 ns/channel for samples containing DAPI
12 and EB alone and 0.1114 ns/channel for EB plus DNA containing samples. Ludox® (from Sigma-
13 Aldrich) was used as the scatter to obtain the instrumental response function. The background
14 (obtained with the blank sample) was subtracted from the decay. The program TRFA data processor
15 version 1.4 (Minsk, Belarus) was used for the analysis of the experimental fluorescence decays. The
16 fluorescence intensity decay over time is described by a sum of exponentials, *i.e*

17
$$I(t) = \sum_{i=1}^{n} \alpha_i \exp\left(\frac{-t}{\tau_i}\right) \quad (2)$$

18 where α_i and τ_i are the normalized amplitude and lifetime of component *i* respectively. From these
19 parameters, the fraction of emitted light by each component *i* can be calculated through

20
$$f_i = \frac{\alpha_i \tau_i}{\sum(\alpha_i \tau_i)} \quad (3)$$

21 and changes in the quantum yield by processes affecting fluorescence lifetime are evaluated from the
22 amplitude-weighted average fluorescence lifetime, which is given by

23
$$\tau_{av} = \sum \alpha_i \tau_i \quad (4)$$

24 where α_i and τ_i have the same meaning as in (2). The quality of the fit was judged from a χ^2_R value
25 close to 1.0 and a random distribution of weighted residuals.
26
27 *4.5. Cell studies*
28
29 *4.5.1. Cell culture and cytotoxicity*
30
31 The cytotoxicity of the two complexes for a 24 h incubation time was determined against the A2780
32 (human ovarian carcinoma, cisplatin sensitive) cell line. Cells were grown in Roswell Park Memorial
33 Institute medium (RPMI-1640), supplemented with 10% fetal bovine serum and 1% antibiotics in a
34 CO_2 incubator (Heraus, Germany) at 37 ºC and humidified atmosphere Cell viability was determined
35 using the MTT colorimetric assay that measures the reduction of yellow 3-(4,5-dimethythiazol-2-yl)-

2,5-diphenyl tetrazolium bromide (MTT) by mitochondrial succinate dehydrogenase to purple formazan product.[35] Since reduction of MTT can only occur in metabolically active cells the level of activity is a measure of the viability of the cells. For this purpose, cells were seeded in 96-well plates in growth media at 20×10^3 cells/well with 200 μL of medium. After 24 h, media were replaced and cells incubated with the compounds tested in aliquots of 200 μL/well. Complexes were first solubilized in DMSO and then in cell medium, and added to final concentrations ranging from 2 nM to 100 μM (complexes). The final concentration of DMSO in cell culture medium was lower than 1% (v/v). After continuous exposure for 24 h (37 ºC/5% CO_2), the medium was discarded and cells incubated with 200 μL of MTT solution in PBS (1.2 mM). After 3-4 h at 37 ºC/5% CO_2, the solution was removed and the purple formazan crystals formed inside the cells dissolved in 200 μL DMSO. Cell viability was assessed by measuring the absorbance at 570 nm in a plate spectrophotometer (PowerWave Xs, Bio-Tek, USA) and calculated for each concentration tested using $\% \ Cell \ viability = [A(sample)_{570} - blank / A(control)_{570} - blank] \times 100$ where A_{sample} represents the absorbance reading from the cells treated with the ruthenium complexes and $A_{control}$ that from the untreated cells, *blank* represents absorvance reading from wells (DMSO only). The cytotoxicity of the compounds was quantified by determining the concentration needed to inhibit tumor cell growth by 50% (IC_{50}), based on non–linear regression analysis of dose-response data using the GraphPad Prism software (vs.4.0).

4.5.2. Mechanisms of cell death: Annexin-V/PI staining

A2780 cells were treated with complexes **1** and **2** at three different concentrations, chosen as the IC_{50} concentration (24 h), one value lower and one above, namely 30 μM, 50 μM and 70 μM for complex **1** and 10 μM, 30 μM and 50 μM for complex **2**.

After treatment with **1** and **2** for 24 h, 1.5×10^6 cells (control) and 3×10^6 cells (test samples for **1** and **2**) were harvested and washed twice with ice-cold PBS. Cells were then re-suspended in 10 μL PI (50 μg/mL) and FITC-conjugated Annexin-V (5 μL) along with binding buffer (pH 7.4 HEPES 0.1 M/1.4 M NaCl/25 mM $CaCl_2$, diluted 1:10 with Millipore® water). After 20 min at room temperature in the dark, cell staining was analyzed by fluorescence-activated cell sorting (FACS) using a Beckman Coulter EPICS XL-MCL. All data was analyzed using WinMDI 2.9 software plotting the fluorescence of PI over Annexin-V fluorescence.

4.5.3. Cell Cycle Analysis

In order to investigate the possible effect of the ruthenium compounds on cell cycle progression by flow cytometry, A2780 cells were treated with **1** and **2** for 24 h. Briefly, 1.5×10^6 (control) and 3×10^6 (**1**

and **2**) cells were harvested washed twice with PBS, fixed with 80% (v/v) cold aqueous ethanol and stored overnight at 4 °C. The fixed cells were washed twice with PBS and incubated with 10 µL of RNase (stock 100 µg/mL) and 10 µL of PI (15 µg/mL). Samples were incubated at 37 °C in the dark and analyzed by flow cytometry (Beckman Coulter EPICS XL-MCL). The percentage of cells in G1/G0, S, G2/M and sub-G1 phases was obtained by univariate models after exclusion of duplets using FlowJo V10 software.

4.5.4. Morphological analysis by TEM

A2780 cells at approximately 70% confluence were treated with **1** and **2** at 50 µM equimolar concentration for 24 h at 37 °C, and untreated cells were used as controls. After incubation cells were processed following a standard procedure used before by some of us and previously reported.[36] Briefly, the culture medium was discarded and replaced by primary fixative consisting of 3% glutaraldehyde in 0.1 M sodium cacodylate buffer pH 7.3. Following primary fixation for 2 h at 4 °C and a wash step in cacodylate buffer, cells were then scrapped, pelleted and embedded in 2% agar for further processing. Samples were further fixed for 3 h in 1% osmium tetroxide in 0.1 M sodium cacodylate buffer pH 7.3. Then, samples were washed in acetate buffer (0.1 M, pH = 5.0) and fixed in 0.5% uranyl acetate in the same buffer for 1 h. Dehydration was carried out with increasing concentrations of ethanol. After passing through propylene oxide, samples were embedded in Epon-Araldite, using SPI-Pon as an Epon 812 substitute. Glass or diamond knives were used to cut thin sections which were stained with 2% aqueous uranyl acetate and Reynold's lead citrate. The stained sections were analyzed and photographed in a JEOL 1200-EX electron microscope.

Appendix. Supplementary data

Supplementary data related to this article can be found online at…

Abbreviations

ctDNA   calf thymus DNA (Deoxyribonucleic acid)

DAPI   4',6-diamidino-2-phenylindole

EB   ethidium bromide

HEPES   4-(2-hydroxyethyl)-1-piperazineethanesulfonic acid

PI   propidium iodide

References

1   N. A. Howlader N, Krapcho M, Garshell J, Neyman N, Altekruse SF, Kosary CL, Yu M, Ruhl J, Tatalovich Z, Cho H, Mariotto A, Lewis DR, Chen HS, Feuer EJ, Cronin KA (eds). , April 2013, pp. Howlader N, Noone AM, Krapcho M, Garshell J, Neyman N, Altekruse SF, Kosary CL, Yu M, Ruhl J, Tatalovich Z, Cho H, Mariotto A, Lewis DR, Chen HS, Feuer EJ, Cronin KA (eds). SEER Cancer Statistics Review, 1975-2010, National Cancer Institute. Bethesda, MD, http://seer.cancer.gov/csr/1975_2010/, based on November 2012 SEER data submission, posted to the SEER web site, April 2013.

2   Ferlay J, Shin HR, Bray F, Forman D, Mathers C and Parkin DM., GLOBOCAN 2008 v2.0, Cancer Incidence and Mortality Worldwide: IARC CancerBase No. 10 Lyon, France: International Agency for Research on Cancer; 2010. Available from: http://globocan.iarc.fr, accessed on 06/06/2016.

3   B. Rosenberg, L. Van Camp and T. Krigas, *Nature*, 1965, **205**, 698–699.

4   L. Kelland, *Nat. Rev. Cancer*, 2007, **7**, 573–584.

5   A. Bergamo, C. Gaiddon, J. H. M. Schellens, J. H. Beijnen and G. Sava, *J. Inorg. Biochem.*, 2012, **106**, 90–99.

6   R. Trondl, P. Heffeter, C. R. Kowol, M. A. Jakupec, W. Berger, B. K. Keppler, *Chem. Sci.*, 2014, **5**, 2925–2932.

7   G. Suss-Fink, *Dalton Trans.*, 2010, **39**, 1673–1688.

8   A. Levina, A. Mitra and P. A. Lay, *Metallomics*, 2009, **1**, 458–470.

9   T. S. Morais, A. Valente, A. I. Tomaz, F. Marques, M. Helena Garcia, *Future Med. Chem.*, 2016, **8**(5), 527-544.

10   A. I. Tomaz, T. Jakusch, T. S. Morais, F. Marques, R. F. M. de Almeida, F. Mendes, É. A. Enyedy, I. Santos, J. C. Pessoa, T. Kiss and M. H. Garcia, *J. Inorg. Biochem.*, 2012, **117**, 261–269.

11   A. Valente, M. H. Garcia, F. Marques, Y. Miao, C. Rousseau and P. Zinck, *J. Inorg. Biochem.*, 2013, **127**, 79–81.

12   F. Kratz, *J. Controlled Release*, 2008, **132**, 171–183.

13   J. C. Pessoa and I. Tomaz, *Curr. Med. Chem.*, 2010, **17**, 3701–3738.

14   K. Vermeulen, D. R. Van Bockstaele and Z. N. Berneman, *Cell Prolif.*, 2003, **36**, 131–149.

15   C. P. Matos, A. Valente, F. Marques, P. Adão, M. P. Robalo, R. F. M. de Almeida, J. C. Pessoa, I. Santos, M. H. Garcia and A. I. Tomaz, *Inorg. Chim. Acta*, 2013, **394**, 616–626.

16   M. J. Waring, *J. Mol. Biol.*, 1965, **13**, 269–282.

17   B. S. P. Reddy, S. M. Sondhi and J. W. Lown, *Pharmacol. Ther.*, 1999, **84**, 1–111.

18   J. R. Lakowicz, *Principles of Fluorescence Spectroscopy*, Springer, 2006.

19 L. Zékány and I. Nagypál, in *Computational Methods for the Determination of Stability Constants*, ed. D. L. Leggett, Plenum Press, New York, 1985, p. 291.

20 O. Dömötör, C. G. Hartinger, A. Bytzek, T. Kiss, B. Keppler and E. A. Enyedy, *J. Biol. Inorg. Chem.*, 2013, **18**, 9–17.

21 É. A. Enyedy, L. Horváth, A. Hetényi, T. Tuccinardi, C. G. Hartinger, B. K. Keppler and T. Kiss, *Bioorg. Med. Chem.*, 2011, **19**, 4202–4210.

22 J.-L. Butour and J.-P. Macquet, *Eur. J. Biochem.*, 1977, **78**, 455–463.

23 C. Liu, J. Zhou and H. Xu, *J. Inorg. Biochem.*, 1998, **71**, 1–6.

24 D. Banerjee and S. K. Pal, *J. Phys. Chem. B*, 2008, **112**, 1016–1021.

25 Y. Kubota, K. Kubota and S. Tani, *Nucleic Acids Symp. Ser.*, 2000, **44**, 53–54.

26 S. Eriksson, S. K. Kim, M. Kubista and B. Norden, *Biochemistry*, 1993, **32**, 2987–2998.

27 H.-X. Zhang, X. Huang, P. Mei, K.-H. Li and C.-N. Yan, *J. Fluoresc*., 2006, **16**, 287–294.

28 H. A. Benesi and J. H. Hildebrand, *J. Am. Chem. Soc.*, 1949, **71**, 2703–2707.

29 A. Wolfe, G. H. Shimer and T. Meehan, *Biochemistry*, 1987, **26**, 6392–6396.

30 U. K. Komarnicka, R. Starosta, M. Płotek, R. F. M. de Almeida, M. Jeżowska-Bojczuk and A. Kyzioł, *Dalton Trans.*, 2016, **45**, 5052–5063.

31 E.P. Bastos, S. Scolari, M. Stöckl, R.F.M. de Almeida, *Methods Enzymol.*, 2012, **504**, 57–81.

32 Mukherjee S, Chiu R, Leung SM, Shields D. *Traffic*., 2007 **8**, 369–378.

33 M. Chiara Maiuri, Einat Zalckvar, Adi Kimchi and Guido Kroemer, *Nat. Rev. Mol. Cell Biol.*, 2007, **8**, 741–752.

34 S.R. Gallagher, *Quantitaion of DNA and RNA with absorption and fluorescence spectroscopy*, in *Current Protocols in Molecular Biology*, ed. F.M. Ausubel, Greene and Wiley-Interscience, New York, 1994.

35 T. Mosmann, *J. Immunol. Methods*, 1983, **65**, 55–63.

36 T. S. Morais, Filipa C. Santos, Tiago F. Jorge, Leonor Côrte-Real, Paulo J. Amorim Madeira, Fernanda Marques, M. Paula Robalo, António Matos, Isabel Santos and M. H. Garcia, *J. Inorg. Biochem.*, 2014, **130**, 1–14.